Compressibility of natural manganite at high pressure: Influence of Jahn–Teller effect and hydrogen bond

Article *in* High Temperatures-High Pressures · May 2017

CITATIONS
0

READS
128

8 authors, including:

Dongyu Zhao
Chinese Academy of Sciences
3 PUBLICATIONS **1** CITATION
SEE PROFILE

Jingui Xu
Chinese Academy of Sciences
18 PUBLICATIONS **36** CITATIONS
SEE PROFILE

Dawei Fan
Chinese Academy of Sciences
60 PUBLICATIONS **191** CITATIONS
SEE PROFILE

Zhou Wen-Ge
Chinese Academy of Sciences
63 PUBLICATIONS **411** CITATIONS
SEE PROFILE

High Temperatures-High Pressures, Vol. 46, pp. 61–79
Reprints available directly from the publisher
Photocopying permitted by license only

Compressibility of natural manganite at high pressure: Influence of Jahn-Teller effect and hydrogen bond

Dongyu Zhao[1,2], Jingui Xu[1,2], Bo Zhang[1,2], Yunqian Kuang[1,2], Dawei Fan[1], Wenge Zhou[1,*], Xiaodong Li[3] and Hongsen Xie[1]

[1]*Key Laboratory for High Temperature and High Pressure Study of the Earth's Interior, Institute of Geochemistry, Chinese Academy of Sciences, Guiyang 550002, China*
[2]*University of Chinese Academy of Sciences, Beijing 100049, China*
[3]*Beijing Synchrotron Radiation Facility, Institute of High Energy Physics, Chinese Academy of Sciences, Beijing 100049, China*

Received: March 17, 2016. Accepted: May 3, 2016.

The pressure-volume relations of a natural manganite [γ-MnOOH] were measured at ambient temperature and high pressures up to 12.7 GPa using a diamond anvil cell (DAC) equipment and synchrotron radiation X-ray diffraction technique. No phase transition has been observed within the whole pressure range in this study. Analysis of pressure-volume data on $P2_1/c$ setting structure to a third-order Birch-Murnaghan equation of state yielded: zero-pressure volume $V_0 = 135.46(4)$ Å^3, isothermal bulk modulus $K_0 = 86(2)$ GPa and its pressure derivative $K'_0 = 6.8(6)$. The axial compression behavior shows that the manganite is a compression anisotropic mineral with $K_{a0} = 93(4)$ GPa, $K_{b0} = 62(5)$ GPa, $K_{c0} = 82(4)$ GPa, which reveals that the *a*-axis is the least compressible, then *b*-axis is the most compressible, and *c*-axis is between them. Comparing the compressibility of manganite based on $P2_1/c$ with $B2_1/d$ setting showed that the different of crystallization orientation was the unique reason for the different axial modulus. Furthermore, we also compared the compressional properties manganite with pyrolusite (β-MnO_2) and the hydroxides of InOOH-related structure which were isotopological to manganite ($B2_1/d$), and inferred that the combinations of Jahn-Teller effect and hydroxyl were the major reasons for the far less bulk modulus of manganite than that of the pyrolusite, and the Jahn-Teller effect and the least electronegativity

*Corresponding author: zhouwenge@vip.gyig.ac.cn

central coordinated cation-Mn^{3+} in manganite were the reasons for having the smallest bulk modulus of manganite among the InOOH-related hydroxides.

Keywords High-pressure, Natural manganite, X-ray diffraction, Equation of state, Jahn-Teller effect

1 INTRODUCTION

Hydroxide group mineral-$M^{3+}OOH$ (M^{3+} is trivalent cation) could be divided into two series according to the type of cations. The central coordination ions of hydroxide group mineral-$M^{3+}OOH$ are seven-fold coordinated without strong hydrogen bonds when the trivalent cations (M^{3+}) are Ho^{3+}, Tb^{3+}, Yb^{3+}, Lu^{3+}, Er^{3+}, Y^{3+}. However, the central coordination ions of hydroxide group mineral-$M^{3+}OOH$ are the octahedral-coordination with strong hydrogen bonds when the trivalent cations (M^{3+}) are Al^{3+}, Cr^{3+}, Mn^{3+}, Fe^{3+}, Ga^{3+}, In^{3+}, Co^{3+}, Ni^{3+}, in this case, the hydroxide group minerals of the octahedral-coordination can be also called InOOH-related hydroxides [1–3]. Manganite is an oxyhydroxide of manganese and belongs to the octahedral-coordination hydroxide mentioned above. The manganite has a monoclinic structure with chemical formula [γ-MnOOH], which is one of the natural polymorphs of $Mn^{3+}OOH$ and the other two polymorphs are orthorhombic groutite [α-MnOOH] and hexagonal feitknechtite [β-MnOOH]. Garrido [4] first described the crystal structure model of manganite and thought manganite belongs to orthorhombic crystal system. Furthermore, Garrido [4] also believed that the manganite has the similar structure with marcasite (FeAsS) which also belongs to the AB_2-type structural minerals. However, Buerger [5] considered that the manganite should be the AB*'* B*"* type structural mineral which is similar to the crystal structure of arsenopyrite (monoclinic, $B2_1/d$ or $P2_1/c$, a super structure of marcasite) rather than AB_2 type structure because of the existence of hydrogen bond in manganite can produce two kinds of O sites (B*'* and B*"*). Nowadays, although it is generally believed that the manganite is a monoclinic structural mineral [2–3, 5–7], there is still not yet a consistent understanding about its space group.

To date, the structure analysis of manganite is carried out based on two species of space group, $P2_1/c$ (standard space group) and $B2_1/d$ (nonstandard space group). The *B*-lattice space group can be transformed to the *P*-lattice space group using a transformation matrix (-1/2 0 1/2; 0 1 0; 1/2 0 1/2). Buerger [6] and Suzuki [3] analyzed the crystal structure of manganite according to the $B2_1/d$ space group mainly due to the monoclinic with $B2_1/d$ setting structure has similar crystallographic axial orientations with the orthorhombic or tetragonal structural minerals, which could be easily compared with orthorhombic structural minerals such as marcasite and other InOOH-related type of hydroxides, as well as tetragonal structural minerals such as

pyrolusite. On the contrary, Kohler et al. [2] analyzed the manganite structure based on the $P2_1/c$ setting (the standard setting).

Recent studies have shown that diaspore (α-AlOOH) as well as its high pressure polymorph (δ-AlOOH) can remain stable at the P-T condition of Earth's mantle, so they may be the important water reservoirs in the deep Earth [8–12]. For example, Friedrich et al. [13] showed that diaspore may stay stable at the pressure up to about 15 GPa and temperature up to 1123 K. Ohtani et al. [9] also indicated that the high-pressure phase of diaspore (α-AlOOH) could stably exist at the pressure from 18 to 116 GPa and the maximum temperature up to 2000 K. Moreover, the diaspore can react with the stishovite to form an important water-bearing minerals assemblage in the mantle-EGG phase [14–15]. In addition, both of manganite and diaspore are InOOH-related hydroxides and have similarity topological properties. Thus, the manganite might be carried into deep Earth accompanied with the subduction of the cold plate under low geothermal gradient [16]. Therefore, the studies about the stability and elastic properties of manganite at high pressure may extremely significant to further understanding the elasticity and aquosity of deep substance as well as water cycling in the deep Earth.

Up to now, only Suzuki [3] studied the high-pressure elasticity of manganite based on the $B2_1/d$ space group. However, studying the high-pressure elasticity of manganite based on the $P2_1/c$ space group setting should be more reasonable because the $P2_1/c$ space group is the standard space group structure according to Kohler et al. [2]. Therefore, here, we investigated the compressibility of natural manganite based on $P2_1/c$ space group setting at room temperature and high pressure in a diamond anvil cell using *in situ* angle-dispersive X-ray synchrotron powder diffraction, and discussed the different of elastic behavior of manganite based on $P2_1/c$ and $B2_1/d$ setting respectively. Moreover, we also compared the compressibility of manganite with pyrolusite and InOOH-related structural hydroxides, and inferred the possible reasons for the different elastic properties among them.

2 SAMPLE AND EXPERIMENTAL METHOD

The natural manganite sample used in this study was collected from Harz of Thuringia, Germany. The chemical formulas of the sample were calculated to be $Mn_{0.995}Fe_{0.002}Ca_{0.001}Cr_{0.001}Ni_{0.001}O(OH)$ based on the results of electron microprobe analysis (Tab. 1). The relatively pure manganite samples were selected by hand under a microscope, and then grounded in an agate mortar for 4–6 hours to obtain an average grain size about 10 μm, which were mixed with 1wt.% Au powder and grounded again for approximately 4–6 hours. The grounded mixed powder samples were then heated at 50°C in constant temperature furnace to remove the absorbed water.

TABLE 1
The chemical composition of manganite (wt%)

	FeO	**SiO_2**	**Cr_2O_3**	**MgO**	**MnO**	**CaO**	**Al_2O_3**	**NiO**	**Total**
Manganite (4)[a]	0.170 (45)	0.008 (5)	0.099 (94)	0.021 (21)	74.628 (284)	0.051 (13)	0.018 (12)	0.042 (11)	75.011 (217)

Data in the parentheses of compositions represent standard deviation.
[a]The number of electron microprobe analyses in parentheses.

In situ high-pressure angle-dispersive X-ray diffraction experiment of natural manganite was conducted at the 4W2 beamline of the Beijing Synchrotron Radiation Facility (BSRF). The wavelength of the monochromatic X-ray beam is 0.6199 Å calibrated by scanning through the Mo metal *K*-absorption edge. The distance between was focused to a beam size of $20 \times 30\,\mu m^2$ full width at half maximum by a pair of Kirkpatrick–Baez mirrors. The tilting and rotation of the detector relative to the incident X-ray beam was calibrated using cerium dioxide (CeO_2) powder as the X-ray diffraction standard. The sample-detector distance was calculated from the powder CeO_2 diffraction pattern at ambient conditions. The high-pressure and room-temperature experiments were carried out using a Piston Cylinder "Mao type" symmetric diamond anvil cell equipping with two diamond anvils (culet faces diameter 500 μm) [17]. A T301 steel gasket with an initial thickness of 200 μm was pre-indented to the thickness of about 50 μm, and then a 200 μm diameter hole was drilled in the center of pre-indentation to be used as a sample chamber. The pressure transmitting medium was a mixture (16:3:1) of methanol-ethanol-water and the gold was a material of pressure calibration based on the equation of state of gold [18]. An image plate detector MAR-345 was used to collect the diffraction patterns. Typical exposure times for collecting diffraction patterns of the sample and the pressure marker were 600 s. The diffraction patterns were integrated to generate the conventional 1-D profiles using the Fit2D program [19]. The natural manganite usually has poor crystalline, and coexists with pyrolusite, ramsdellite and psilomelane and all of them have the similar physical properties [20]. Therefore, the X-ray diffraction patterns of natural manganite always shows the character of scarce diffraction peaks, poor profiles and mixing impurity peaks.

As mentioned above, the crystal structure of manganite can be analyzed based on two types of settings ($B2_1/d$ and $P2_1/c$). Here, we identified the diffraction peaks of manganite based on the $P2_1/c$ space group (*ICSD#*:084949; [2]) and $B2_1/d$ space group (*ICSD*#:027457; [7]) respectively, and got the diffraction peaks of manganite ($\bar{1}11$), (020)/($\bar{1}02$), (111), (002)/(200), ($\bar{1}21$), (-202), (210)/(012), ($\bar{2}21$)/($\bar{1}22$), (022)/(220), ($\bar{3}02$)/($\bar{2}22$), ($\bar{3}11$)/($\bar{1}13$), ($\bar{1}31$) based on the standard diffraction pattern of $P2_1/c$ space group (Fig. 1(a)), and the diffraction peaks (210), (020), (012), (-202)/(202), (220), (400), ($\bar{2}12$)/(212), (321)/($\bar{3}21$), ($\bar{2}22$)/(222), (420), ($\bar{4}12$)/(412), (230) according to

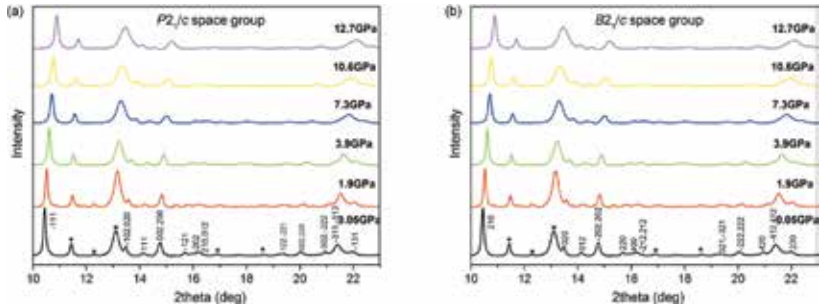

FIGURE 1
Representative one-dimensional X-ray diffraction patterns of manganite obtained in this study at room temperature and pressure up to 12.7GPa. The *stars* mean that the impurity diffraction peaks which couldn't be indexed reasonably. **(a)** Indexation based on the standard diffraction pattern of $P2_1/c$ space group (*ICSD#*:084949; [2]). **(b)** Indexation based on the nonstandard diffraction pattern of $B2_1/d$ space group(*ICSD#*:027457; [7]).

the $B2_1/d$ space group (Fig. 1(b)). The diffraction peak positions were determined using a peak fitting program. And then the cell parameters of manganite were calculated and refined by using the UnitCell process [21]. Here in after we will mainly discuss the elasticity of manganite based on $P2_1/c$ setting.

3 RESULTS

The experimental pressure was gradually increased up to 12.7 GPa. The typical diffraction patterns selected at various pressures are shown in Fig. 1. The diffraction peaks marked with stars are the diffraction lines could not be indexed reasonably by standard patterns of manganite (*ICSD#*: 084949; [2]) and (*ICSD#*: 027457; [7]), which might be the mixing of impurity diffraction peaks of other oxides or hydroxides of manganese (pyrolusite, ramsdellite, psilomelane, etc.), while other diffraction peaks belong to the manganite. Furthermore, no phase transition was observed in the pressure range explored. As pressure increased, all the peaks shifted continuously toward higher 2θ and the diffraction lines broaden and weaken slightly, but the overall pattern did not change (Fig. 1). The pressure dependency of the *d*-spacings of manganite based on $P2_1/c$ setting is shown in Fig. 2, which shows a continuous decrease with the increase in pressure, indicating that the sample is stable up to 12.7 GPa. The *d*-spacing of (–111), (020), (002), (–311) diffraction reflections that were prominent, non-overlapping, and observable until the end of the experiment are shown.

Table 2 summarizes the unit-cell parameters of manganite at different pressure obtained from this study based on the $P2_1/c$ and $B2_1/d$ settings,

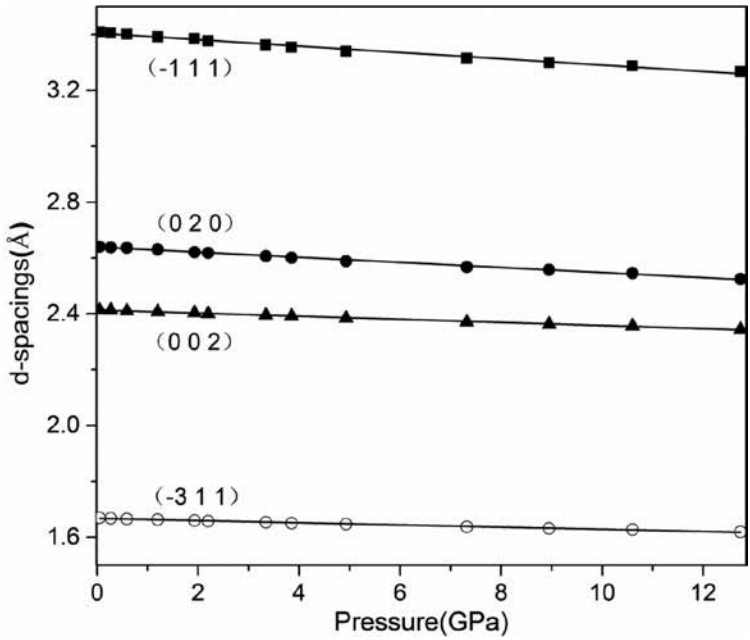

FIGURE 2
Variation of characteristic *d*-spacings of manganite ($P2_1/c$ space group) with pressure. The *solid lines* are linear fitting of the data.

TABLE 2
Cell parameters versus pressure for manganite ($P2_1/c$ and $B2_1/d$ space group)

	$P2_1/c$ space group					***$B2_1/d$ space group***				
P(GPa)	*a*(Å)	*b*(Å)	*c*(Å)	*β*(°)	*V*(Å^3)	*a*(Å)	*b*(Å)	*c*(Å)	*β*(°)	*V*(Å^3)
0.05	5.299(1)	5.285(2)	5.304(2)	114.42(4)	135.24(6)	8.913(4)	5.285(3)	5.742(3)	89.94(3)	270.4(1)
0.3	5.2944(6)	5.287(1)	5.300(7)	114.43(1)	135.06(2)	8.907(1)	5.287(1)	5.7364(9)	89.933(9)	270.12(5)
0.6	5.288(2)	5.271(3)	5.297(2)	114.41(5)	134.45(8)	8.898(5)	5.271(3)	5.733(4)	89.89(4)	268.9(1)
1.2	5.278(1)	5.260(2)	5.286(1)	114.34(3)	133.71(6)	8.876(3)	5.260(2)	5.727(2)	89.91(2)	267.4(1)
1.9	5.268(2)	5.249(3)	5.268(2)	114.21(4)	132.87(7)	8.847(5)	5.249(3)	5.722(3)	90.00(4)	265.7(1)
2.2	5.261(1)	5.242(2)	5.262(2)	114.24(5)	132.32(7)	8.837(6)	5.242(3)	5.713(5)	90.00(4)	264.6(1)
3.3	5.245(2)	5.212(2)	5.242(2)	114.02(4)	130.89(7)	8.796(4)	5.212(3)	5.710(3)	90.04(3)	261.8(1)
3.9	5.236(1)	5.200(2)	5.230(2)	113.90(6)	130.18(7)	8.773(4)	5.200(3)	5.708(4)	90.06(3)	260.4(1)
4.9	5.224(1)	5.178(2)	5.206(2)	113.76(5)	128.90(7)	8.735(5)	5.178(3)	5.699(4)	90.22(3)	257.8(1)
7.3	5.192(1)	5.146(2)	5.166(2)	113.42(5)	126.67(6)	8.659(4)	5.146(2)	5.686(4)	90.31(2)	253.3(1)
9.0	5.178(2)	5.115(3)	5.148(3)	113.45(9)	125.0(1)	8.633(7)	5.115(4)	5.665(6)	90.37(4)	250.1(2)
10.6	5.163(3)	5.092(5)	5.126(4)	113.2(1)	123.8(1)	8.591(9)	5.092(5)	5.663(8)	90.44(6)	247.7(2)
12.7	5.136(4)	5.071(8)	5.088(5)	113.0(1)	122.0(1)	8.53(1)	5.071(8)	5.64(1)	90.59(8)	243.9(3)

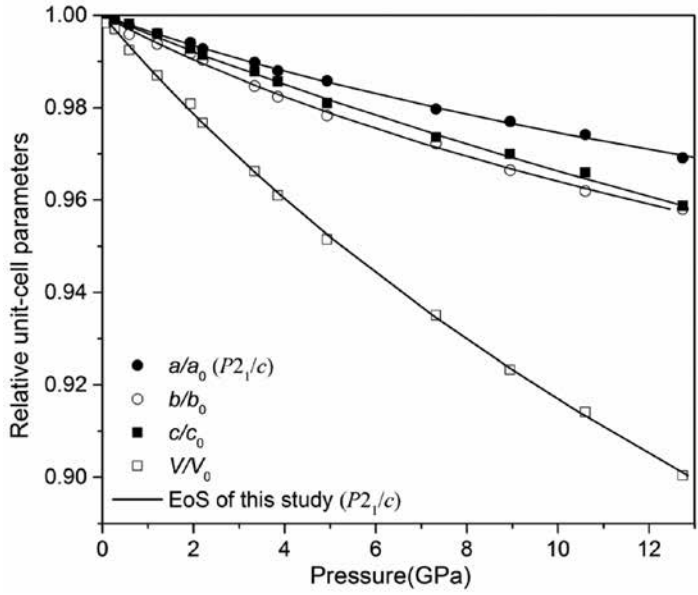

FIGURE 3
Pressure-volume and unit cell parameters *a b c* data of $P2_1/c$ setting manganite. A third Birch-Murnaghan equation of state fitted with *solid curves*. The size of the *symbols* exceeds the *error bars*.

respectively. The evolution of the lattice parameters for the manganite (V/V_0, a/a_0, b/b_0, c/c_0) with pressure, based on the powder X-ray diffraction data in this study, is shown in Fig. 3. Unit-cell volume data were fitted with a third-order Birch-Murnaghan equation of state [22] using the EoS-FIT5.2 program [23]:

$$P = (3/2)\, K_0\, [(V_0/V)^{7/3} - (V_0/V)^{5/3}] \times \{1+(3/4)\,(K'_0-4)\,[(V_0/V)^{2/3}-1]\} \quad (1)$$

where V_0, K_0, K'_0 are the zero-pressure volume, high-pressure volume, zero-pressure isothermal bulk modulus and its pressure derivative, respectively. The elastic parameters, simultaneously refined using the data weighted by the uncertainties in P and V, are $V_0 = 135.46(4)$ Å^3, $K_0 = 86(2)$ GPa, and $K'_0 = 6.8(6)$.

To assess the quality of the Birch-Murnaghan EoS fit obtain from the plot of unit cell volume against pressure, the relationship between the Eulerian strain ($f_E = [(V_0/V)^{2/3}-1]/2$) and "normalized pressure" ($F_E = P/[3f_E(2f_E+1)^{5/2}]$) was plotted, and shown in Fig. 5 [24]. The f_E-F_E plot provides a visual indication of which higher order terms, such as K'_0 and K''_0, is significant in the EoS. The manganite data showed a relatively large positive slope (Fig. 5). This indicates that the pressure derivative of the bulk modulus (K'_0) was

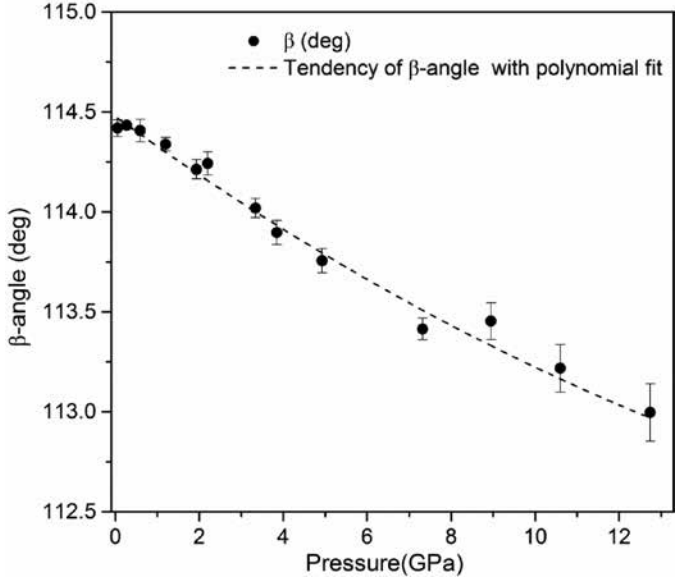

FIGURE 4
P-β data of manganite ($P2_1/c$ setting). The*dotted line* is the result of a second-polynomial fitting.

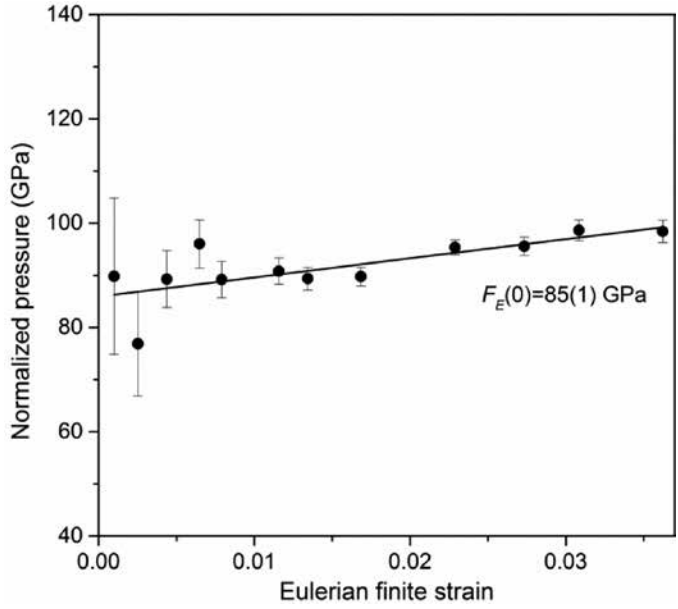

FIGURE 5
Eulerian strain-normalized pressure (*f*-*F*) plot of the data based on the third-order Birch-Murnaghan equation of state. The *solid line* represents the linear fitting of data point.

higher than 4. Therefore, the value, estimated to be 6.8, was consistent with the f_E–F_E plot analysis.

Axial bulk moduli of manganite were also calculated with a "linearized" BM-EoS [24]. The refined elastic parameters are as follows: $a_0 = 5.2995(6)$ Å, $K_{a0} = 93(4)$ GPa with $K'_{a0} = 4$ (fixed) for the a-axis; $b_0 = 5.293(2)$ Å, $K_{b0} = 62(5)$ GPa, with $K'_{b0} = 4$ (fixed) for the b-axis; $c_0 = 5.307(1)$ Å, $K_{c0} = 82(4)$ GPa with $K'_{c0} = 4$ (fixed) for the c-axis [$\beta(a) = 1/3\,K_{a0} = 0.0036(1)\,\text{GPa}^{-1}$; $\beta(b) = 1/3K_{b0} = 0.0054(2)\,\text{GPa}^{-1}$; $\beta(c) = 1/3\,K_{c0} = 0.0041(1)\,\text{GPa}^{-1}$; $\beta(a)$: $\beta(b)$: $\beta(c) = 1{:}1.50{:}1.14$].

In addition, the β-angle of manganite decreases gradually with the increasing pressure (Fig. 4), with $\beta = -0.15(1) \times P + 0.003(1) \times P^2 + 114.18(1)$ (the result of polynomial fit). Compared the results in this study with the previous studies, we can find that arsenopyrite has similar lattice type with manganite (monoclinic with $P2_1/c$ space group), but the β-angle of arsenopyrite increases along with pressure [25] which is different from manganite (monoclinic $P2_1/c$ space group). Similarly, for hollandite ($I2/m$), romanechite ($C2/m$) and todorokite ($P2/m$), which have different lattice type compared with manganite, all of them also show the different relationship between β-angle and pressure compared with manganite in this study. The hollandite and romanechite show that the β-angle gradually increases with pressure, but the todorokite performs that the β-angle increases firstly and then decreases with pressure [26]. Therefore, the descriptions above can explain that both of composition and lattice type of minerals play a vital role in the compression direction of minerals, and then cause the different relationship between β-angle and pressure.

4 DISCUSSION

4.1 Elasticity of manganite based on $P2_1/c$ and $B2_1/d$ setting

In the manganite crystal structure, an octahedral-coordinated basic unit (MnO_6) is formed by one Mn^{3+} ions surrounded by six O^{2-} ions. Strong structural distortion occurs in the coordinated octahedron (MnO_6) because of the combination of Jahn-Teller effect and hydrogen [2–3, 20], which produce two long bonds along the long-axial orientation and four short bonds along the short-axial direction. The closest octahedrons that shares edges or vertices forms the single-chains with 1×1 tunnel structure (the length of every side of the square area is composed of a MnO_6 respectively) in three-dimensional framework. The hydroxyl lays in the vacancy of the tunnel structure in manganite (Fig. 6 (a) and (b)).

The manganite is usually analyzed based on $P2_1/c$ or $B2_1/d$ setting. The $P2_1/c$ setting is a standard setting, which has a secondary screw axis accompanying with an axial glide plane c, primitive lattice, while the $B2_1/d$ setting is a nonstandard setting, having a secondary screw axis accompanying with an

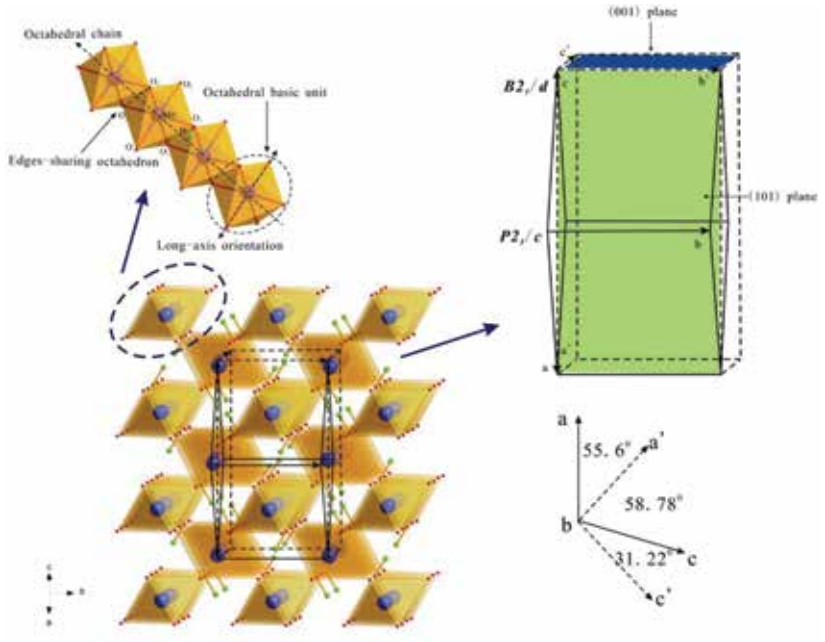

FIGURE 6
(a) Crystal structure of manganite at ambition pressure and room temperature. **(b)** One of the edges-sharing octahedral chain in manganite crystal structure. **(c)** The unit cell edge of $P2_1/c$ and $B2_1/d$ setting manganite, while the *solid line* and the *dotted line* represent the unit cell of $P2_1/c$ and $B2_1/d$ setting manganite respectively. The crystallographic axis of $P2_1/c$ space group cell are *a*, *b* and *c* orientations separately, while the $B2_1/d$ setting are *a'*, *b'* and *c'* direction which is equivalent to the crystal edge of [10$\bar{1}$], *b*and [101] in $P2_1/c$ setting manganite respectively. **(d)** The relative orientations of crystallographic axes of unit cell in manganite based on $P2_1/c$ and $B2_1/d$ setting. The *b* axis is coincide with *b'*, which both perpendicular to the plane direction.

axial glide plane *d*, body-centered lattice. However, the *B*-lattice setting can be transformed to *P*-lattice setting. Most of previous studies analyzed the structure of manganite based on $B2_1/d$ space group just because the monoclinic with $B2_1/d$ setting (pseudo-orthorhombic) was similar to the crystal structure of tetragonal, which was easy to compare with each other [3, 6]. The β-angle is approximately 90° in the structure of monoclinic with $B2_1/d$ space group, causing the similar crystal axial orientation with the orthorhombic and tetragonal structure. For instance, the unit cell of tetragonal with $P4_2/mnm$ space group is equivalent to a subcell of the monoclinic with $B2_1/d$ setting [2] (Kohler et al. 1997); orthorhombic with *Pnnm* setting structure is equal to the half of the unit cell structure [6] (Buerger 1936a); orthorhombic with $P2_1nm$ structural InOOH-related hydroxide (δ-AlOOH, ε-FeOOH, β-CrOOH etc.) have the similar crystal axial direction with the manganite based on $B2_1/d$ setting [3].

The different of two types of unit cell structures based on different settings in manganite is actually the difference in crystal orientation (crystal axial

direction) as shown in Fig. 6 (c) and (d). The manganite has a body-lattice structure with $\beta = 90°$ in the $B2_1/d$ setting structure. The *c'*-axis orientation along with the direction of a single-chain linkage. The hydroxyl is located in the tunnel structure and parallel to the plane (001) that is made up of the *a'*- and *c'*-axis (Fig. 6 (a) and (c)). However, the lattice type is primitive lattice with $\beta \neq 90°$ in the $P2_1/c$ setting structural manganite and the single-chain of coordinated octahedron MnO_6 is perpendicular to the (101) plane of tunnel structure where hydroxyl located (Fig. 6 (a) and (c)).

Due to the $B2_1/d$ setting can be transformed to $P2_1/c$ setting, the direction of *a*-, *b*- and *c*-axis is equivalent to the crystallographic axis of [10$\bar{1}$], *b* and [101] respectively (Fig. 6 (b)). Based on $P2_1/c$ setting, the calculated bulk modulus of manganite is $K_0 = 86(2)$ GPa and the axial moduli of manganite are $K_{a0} = 93(4)$ GPa, $K_{b0} = 62(5)$ GPa and $K_{c0} = 82(4)$ GPa, respectively, however, based on $B2_1/d$ setting, the bulk modulus and axial moduli of manganite are $K_0 = 86(4)$ GPa, $K_{a'0} = 72(3)$ GPa, $K_{b'0} = 62(5)$ GPa, $K_{c'0} = 199(24)$ GPa, respectively. Although the manganite can be analyzed by above mentioned two types of space group ($P2_1/c$ and $B2_1/d$ setting), both of them have the same bulk modulus value. Moreover, both of the $P2_1/c$ and $B2_1/d$ setting have the similar *b*-axial orientation, so the calculated axial moduli of *b*-axis based on $P2_1/c$ and $B2_1/d$ settings are also the same. However, the axial moduli of *a*- and *c*-axis are totally different between the $P2_1/c$ and $B2_1/d$ setting. In addition, it is worth to say that *a'*-, *b'*-, and *c'*-axis of manganite in $B2_1/d$ crystal structure are equivalent to the [10$\bar{1}$], *b* and [101] axial directions in $P2_1/c$ crystal structure. Therefore, the axial moduli of manganite base on $B2_1/d$ setting are equal to that of [10$\bar{1}$], *b* and [101] direction based on $P2_1/c$ setting (Fig. 6 (b), Tab. 3).

Recently, Suzuki [3] studied the elasticity of manganite up to 10.1GPa at room temperature based on $B2_1/d$ setting. Table 2 shows the comparison of the bulk modulus and axial moduli in this study according to $B2_1/d$ setting with the value of Suzuki [3]. From table 2, we can find that the bulk modulus [86(4) GPa] and axial moduli values of manganite [$K_{a0} = 72(3)$ GPa, $K_{b0} = 62(5)$ GPa, $K_{c0} = 199(24)$ GPa; $B2_1/d$ setting] obtained in this study are similar to the data of Suzuki [3] [$K_0 = 91(3)$ GPa, $K_{a'0} = 67(6)$ GPa, $K_{b'0} = 67(5)$ GPa, $K_{c'0} = 219(48)$ GPa] within their uncertainties (Tab. 3, Fig. 7 (a) (b) (c) (d)).

TABLE 3
Bulk moduli of manganite. The axial moduli of *a'*-, *b'*-and *c'*axis with $B2_1/d$ setting manganite are equivalent to the crystal edge of [10$\bar{1}$], *b*and [101] with $P2_1/c$ setting respectively

Space groups	V_0(Å^3)	K_0(GPa)	K'_0	$K_{a0}(K_{a'0})$ (GPa)	$K_{b0}(K_{b'0})$ (GPa)	$K_{c0}(K_{c'0})$ (GPa)	References
$B2_1/d$	270.47(9)	91(3)	7(1)	67(6)	67(5)	219(48)	Suzuki [3]
$B2_1/d$	270.93(16)	86(4)	6.8(11)	72(3)	62(5)	199(24)	This study
$P2_1/c$	135.24(6)	86(2)	6.8(6)	93(4)	62(5)	82(4)	This study

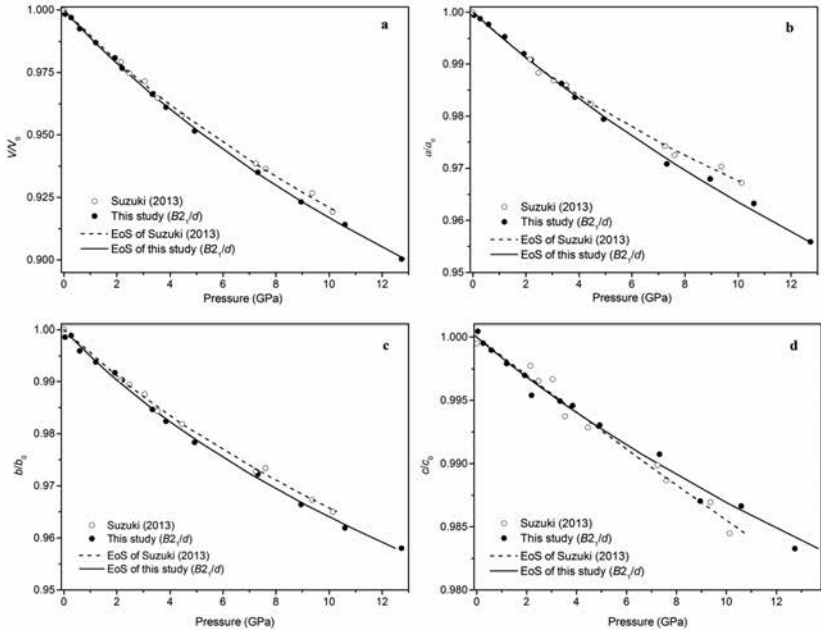

FIGURE 7
Comparative the data of $B2_1/d$ setting structural manganite obtained in this study with the study of Suzuki [3]. The *solid* and *dotted curve* all represent the results of a third-order Birch-Murnaghan equation of state. The *error bars* of the data points are smaller than the *symbols.* **(a)** *P-V* data. **(b)** *P-a* data. **(c)** *P-b* data. **(d)** *P-c* data.

Thus, we choice of the standard ($P2_1/c$) or non-standard setting ($B2_1/d$) did not have a significant effect on the parameters derived from the EoS fitting and these agree with one another within experimental error. In addition, the crystal orientations of different settings are not always the same, so it is obviously different in axial compression properties when analyzes the manganite crystal structure according to different space groups. However, the $P2_1/c$ setting is the standard setting in the crystal structure of manganite, so we believe that the study of compression properties of manganite based on $P2_1/c$ setting could reveal the accurately and reasonably compression behavior of manganite.

4.2 Compression anisotropy

The axial compression properties of manganite based on $P2_1/c$ setting are shown in Figure 3. The axial moduli of manganite along *a*-, *b*- and *c*-axis are 93(4) GPa, 62(5) GPa and 82(4) GPa, respectively, which indicates that the manganite is elastic anisotropy (Fig. 3). Manganite has the similar structure with InOOH-related hydroxides, such as δ-AlOOH, which preforms that the linkage of coordinated octahedron is made up with a central ion and six O ions surrounded, and the linkage octahedron shares vertices and edges. It is

generally believed that the octahedron structure is rigid and hard to compress [13, 27]. The study of Friedrich et al. [13] showed that the bulk modulus of AlO_6 [213.9(1) GPa] is larger than δ-AlOOH [143.7(9) GPa]. These indicate that the rigid octahedron of coordinated cation of InOOH-related structure is hard to compress and the compression behavior of InOOH-related hydroxides is more likely to occur at the vacant of hydrogen bonds with pressure.

The axial compression behavior of InOOH-related structural minerals also depends on the distribution of hydroxyl in the crystal structure. Since the strength of hydrogen bonds is much weaker than the ionic bonds and covalent bonds, it is easier to compress along the direction of hydrogen bonds. The distribution of hydroxyl is along with the direction of *b*-axis in the crystal structure of manganite ($P2_1/c$ setting) and parallel to (101) plane in the tunnel structure (Fig. 6a). So the *b*-axial orientation is the most compressible direction in the manganite. The coordinated octahedron that shares vertices and edges and forms series of single chains in the direction that perpendicular to (101) plane. The orientation of octahedron chain of edge-sharing without hydrogen bonds perpendicular to (101) plane is the least compression direction (the *c'*-axis direction of manganite based on $B2_1/d$ setting) on the basics of the properties of rigid octahedron. Due to the combined impact of Jahn-Teller effect and hydrogen bonds, the distortion of MnO_6 octahedron occurs in manganite and the Mn-O bonds produce varying degrees of stretch and compression, so there is a slight discrepancy of the angle between the orientation of edge-sharing octahedral chains with the *a*-and *c*-axial direction, respectively (55.650° and 58.787° [3]). Thus the compression behavior of *a*-axis and *c*-axis in manganite is slightly different.

4.3 Comparison with pyrolusite (β-MnO_2)

Pyrolusite [β-MnO_2] is the corresponding oxide of manganite and belongs to tetragonal with $P4_2/mnm$ space group. The crystal structure of manganite can be viewed that the oxygen ion is displaced by the hydroxyl in the crystal structure of pyrolusite. The Mn^{4+} ion could transform to Mn^{3+} ion while the hydroxyl substitute to oxygen ion in the coordinated octahedron MnO_6 of manganite. The distortion occurs in the octahedron MnO_6 because of Mn^{3+} has strong Jahn-Teller effect, and then reduces the symmetry of crystal structure in manganite. In addition, on account of the ionic radius of hydroxyl (1.37 Å) is far larger than that the oxygen ion (0.74 Å) [28], the distortion of tunnel structure in the crystal structure of manganite may occur when the hydroxyl substitutes the oxygen ion, and may also reduce the symmetry of crystal structure in manganite. Therefore, the manganite is a monoclinic with $P2_1/c$ (or $B2_1/d$) space group mineral.

Pyrolusite belongs to the RO_2-type structural group minerals (R is the quadrivalent cation), which is isostructural with stishovite. Table 4 summarizes the bulk modulus values of pyrolusite, ranging from 187 GPa to 341 GPa [29–31], which is far larger than that the bulk modulus of manganite

TABLE 4
Bulk modulus of pyrolusite

Sample	Structure types	Methods	K_0 (GPa)	K'_0	References
Pyrolusite	$CaCl_2$-type	XRD	328(18) (B-M)	4(2)	Haines et al. [30]
	Cotunnite-type	Theoretical(LDA)	257 (M)	4.40	Dewhurst and Lowther [29]
			330 (B-M)	4.58	
	Rutile-type	Theoretical(DFT)	187		Li et al. [31]
	$CaCl_2$-type		262		
	Pyrite		341		

XRD X-ray diffraction, DFT Calculation based on density functional theory, LDC Calculation based on local density approximation theory, M Fitting based on Murnaghan equation of state, B-M Fitting based on Brich-Murnaghan equation of state.

obtained from this study [86(2) GPa]. The reasons why the bulk modulus value of manganite is much less than the bulk modulus of pyrolusite may be the combination of Jahn-Teller effect and hydrogen bond. The distortion of coordinated octahedron MnO_6 occurs because of the Jahn-Teller effect of Mn^{3+} in manganite. The four Mn-O bonds along the long axis and two Mn-O bonds along the short axis in pyrolusite are 1.8981 Å and 1.8795 Å, respectively [32]. But for manganite, the bond lengths of two Mn-O bonds along the long axis are 2.174(1) Å and 2.338(1) Å, respectively, while the bond lengths of four Mn-O bonds along the short axis are 1.895(1) Å (×2) and 1.965(1) Å (×2), respectively [2]. Compared with pyrolusite, the bond lengths of Mn-O bonds in manganite increase about 12%–18% and 0.8%–4% along the long and short axis direction, respectively. The larger bond length of Mn-O bonds in manganite leads to the expansion of the octahedral unit, and then causes the larger unit cell volume in manganite compared with pyrolusite. Moreover, comparing the cell volume and cell parameters of manganite with that pyrolusite at ambient conditions shows that the cell parameters and cell volume of pyrolusite [$a_0 = 4.437(3)$ Å, $b_0 = 4.312(3)$ Å, $c_0 = 2.862(2)$ Å, $V_0 = 55.48$ Å^3, $Z = 2$] [33] are far less than that of manganite [$a_0 = 5.2995(6)$ Å, $b_0 = 5.293(2)$ Å, $c_0 = 5.307(1)$ Å, $V_0 = 135.46(4)$ Å^3, $Z = 4$]. Hence, compared with pyrolusite, the manganite has more loose crystal structure and much easier to compress.

The influences of hydroxyl on the elastic property of manganite perform in two aspects. First, due to the ionic radius of hydroxyl is larger than that of the oxygen ion, the hydroxyl in the vacant of tunnel structure leads to the expansion of the volume in tunnel structure and then may cause a loosen crystal structure in manganite. Second, the hydrogen bond has weaker strength than other types of bonds (ionic bonds and covalent bonds). Therefore, we infer that the combined impact of Jahn-Teller and hydrogen bond may be the main reason that the bulk modulus of manganite is much less than that of the pyrolusite.

4.4 Comparison with other InOOH-related hydroxides

Manganite [γ-MnOOH] ($B2_1/d$) and diaspore [α-AlOOH], goethite [α-FeOOH], tsumgallite [GaOOH], dzhalindite [InOOH], guyanaite [β-CrOOH] as well as their isomorphic phases belong to the InOOH-related hydroxides, and have similar topological behaviors [2]. In the crystal structure of InOOH-related hydroxides, the trivalent ion of central coordination combined with the surrounded six oxygen ions forms the basic unit of coordinated octahedron which shares the vertices and edges. Hydrogen bond is located at the tunnel structure that is made up with the octahedrons. Table 5 summarizes the bulk modulus of InOOH-related hydroxides. From table 5, we can find that the manganite is the most compressible mineral with the least bulk modulus value 86(2) GPa

TABLE 5
Bulk modulus of representative hydroxides with InOOH-related structure

Samples		Types	Methods	K_0(GPa)	K'_0	Pressure Range(GPa)	References
InOOH related structures	α-AlOOH	nature	XRD	167.5	4(fixed)	0–22.5	Mao et al. [38]
	α-AlOOH	nature	XRD	230	4(fixed)	0–27	Xu et al. [12]
	α-AlOOH	nature	XRD	150(3) (B-M-II)	4(fixed)	0–7	Friedrich et al. [13]
			DFT	150.4(9) (B-M-II)	4(fixed)	7–40	
				143.7(9) (B-M-III)	4.44(6)		
	δ-AlOOH	synthetic	XRD	252(3)	4(fixed)	0–22.5	Vanpeteghem et al. [14]
	δ-AlOOH		DFT	225.5 (HC)	3.3	0–60	Tsuchiya et al. [11]
				182.8 (HOC-I)	4.4		
				186.5 (HOC-II)	4.5		
	δ-AlOOH	synthetic	XRD	124(2)	13.5(7)	0–17	Suzuki [39]
	δ-AlOOH	synthetic	XRD	152(2)	4(fixed)	0–10	Sano-Furukawa et al. [40]
				219(3)		10–63.5	
	β-CrOOH	synthetic	XRD	209(3)	3.5(2)	0–31.2	Sano-Furukawa et al. [41]
	GaOOH	synthetic	XRD	147(3)	7.3(3)	0–35.0	
				157(3)	4(fixed)	0–14.1	
				206(5)	4(fixed)	14.1–35.0	
	InOOH	synthetic	XRD	135(1)	6.7(1)	0–35.2	
				159(2)	4(fixed)	0–15.2	
				192(4)	4(fixed)	15.2–35.2	
	α-FeOOH	nature	XRD	111(2)	4(fixed)	0–24	Nagai et al. [36]
	α-FeOOH	synthetic	XRD	140.3(3.7)	4.6(0.4)	0–29.4	Gleason et al. [42]
	ε-FeOOH			158(5)	4(fixed)		
	ε-FeOOH	synthetic	XRD	126(3)	10(1)	0–11	Suzuki [43]
	γ-MnOOH	nature	XRD	91(3) ($B2_1/d$)	7(1)	0–10.1	Suzuki [3]
		nature	XRD	86(2) ($P2_1/c$)	6.8(6)	0–12.7	This study
				86(4) ($B2_1$/d)	6.8(11)		

XRD X-ray diffraction, DFT Model calculations based on density functional theory, HC, HOC-I andHOC-II are the hydrogen position model. HC (center hydrogen position), HOC-I and HOC-II (two structures with off-centered hydrogen positions). B-M-II Fitting based on second-ordered Birch-Murnaghan equation of state, B-M-III Fitting based on third-ordered Birch-Murnaghan equation of state.

(based on $P2_1/c$ setting) compared with that of other InOOH-type hydroxides (135 GPa–225.5 GPa) (Tab. 5).

It is generally believed that the radius and electronegativity of the central coordinated ion maybe the principal element in affecting the compression properties of the minerals at high-pressure. The efficient ionic radius is larger, and then the electronegativity of the central coordinated ion will be smaller [34]. We also obtain the following relationship: In^{3+}(VI)>Ga^{3+}(VI)>Mn^{3+}(VI) >Fe^{3+}(VI)>Al^{3+}(VI)>Cr^{3+}(VI) (the efficient ionic radius are 0.80 Å, 0.62 Å, 0.58 Å, 0.55 Å, 0.535 Å, 0.49 Å, respectively [28] by comparing the efficient ionic radius of central coordinated ions in InOOH-related hydroxides. Although the central coordinated Mn(VI) ion has not the largest ionic radius, the manganite is the most compressible mineral in the InOOH-related hydroxides. Wei et al. [35] have obtained the same conclusions that the substitution of central coordinated ion with V^{5+}(0.59 Å), As^{5+}(0.46 Å) and P^{5+}(0.35 Å) might have little or no influence on the bulk modulus values of minerals by studying the high-pressure elasticity of vanadinite, pyromorphite and minetisite.

The electronegativity of central coordinated ions in some InOOH-related hydroxides, which have typical isotopological structure, are as follows: Mn(1.55), Al(1.61), Cr(1.66), In(1.78), Ga(1.81), Fe(1.83). Electronegativity is a chemical property that describes the ability of an atom to attract electrons. An atom's electronegativity is affected by its atomic weight and the distance of its valence electrons from the charged nucleus. The higher the associated electronegativity number, the greater the central ions attract electrons, and then form the stronger chemical bonds. Thus, the strength of Mn-O bond in manganite is weaker than that of the M^{3+}-O (the M^{3+} ion is the central coordinated cation in InOOH-related hydroxides) bond in other InOOH-related minerals, which might result in the smaller bulk modulus in manganite than that of other InOOH-related structure minerals. In addition, Xu et al. [34] studied the compressional property of adamite at high pressure and considered that the electronegative of the coordinated ion of Zn, As were weaker than that of Al and Si may be one of the reasons that the bulk modulus of adamite [$Zn_2(AsO_4)OH$] is smaller than that of andalusite [$Al_2(SiO_4)O$]. But the central coordinated octahedral, which composed of the central coordinated M^{3+} and surrounded six oxygen ions in InOOH-related structural hydroxides, is rigid and hard to compress [13, 27, 36–37]. Hence, the compression of the central coordinated octahedron is slight, and the compression of manganite may mainly occur at the location of tunnel structure where hydroxyl exists.

Although the manganite and other InOOH-related hydroxides have similar M^{3+} cation and O^{2-} anion configuration, Mn^{3+}cation in manganite has strong Jahn-Teller effect which is different from other InOOH-type hydroxides. The combination of Jahn-Teller effect and hydrogen bond might result in intense distortion of coordinated octahedron MnO_6 and lower symmetry of manganite. Thus, manganite belongs to monoclinic with $P2_1/c$ space group, which is

different from other InOOH-type hydroxides with orthorhombic structure. The length of M^{3+}-O bonds of typical InOOH-related hydroxide minerals are showed in Table 6. The long-axis of manganite is intensively stretched because of the influence of Jahn-Teller effect, which leads to the largest M^{3+}-O bonds of long-axial of manganite among the InOOH-related hydroxides. The Mn-O bond of long-axis in manganite is about 4%–19% larger than the M^{3+}-O bonds of other InOOH-related hydroxides, while the bonds of short-axis in the coordinated octahedron of manganite are similar to the M^{3+}-O bonds of other InOOH-related hydroxides (Tab. 6). Therefore, compared the coordinated octahedron $M^{3+}O_6$ in other InOOH-related hydroxides, the coordinated octahedron MnO_6 of manganite occur a fierce stretching distortion in the long-axis orientation. So the coordinated octahedron of manganite is much easier to compress than that of other InOOH-related hydroxides. In addition, the fierce stretching distortion in the long-axis orientation of manganite also causes the distortion of tunnel structure, which can expand the volume of tunnel vacant and get a more loose crystal structure of manganite. To sum up, we infer that

TABLE 6
M^{3+}-O data of typical InOOH-related hydroxides (M^{3+} is the center coordination cation)

Representative minerals of InOOH-related	**Bonds**	**Distances Å**	**References**
α-FeOOH	Fe-O1	1.9325(9)	Yang et al. [37]
(Goethite)		1.9560(6) (×2)	
	Fe-O_2	2.0996(9)	
		2.1063(7) (×2)	
α-AlOOH	Al-O_1	1.888	Friedrich et al. [13]
(Diaspore)		1.876 (×2)	
	Al-O_2	1.998	
		1.987 (×2)	
β-CrOOH	Cr-O_1	1.985	Pernet et al. [44]
(Guyanaite)		1.927 (×2)	
	Cr-O_2	2.059	
		2.009 (×2)	
GaOOH	Ga-O_1	1.934	Li et al. [45]
(Tsumgallite)		1.929(×2)	
	Ga-O_2	2.054	
		2.055 (×2)	
InOOH	In-O_1	2.125(3)	Lehmann et al. [46]
(Dzhalindite)		2.138(2) (×2)	
	In-O_2	2.233(3)	
		2.207(3) (×2)	
γ-MnOOH	Mn-O_1	2.337(1)	Kohler et al. [2]
(Manganite)		1.982(1)	
		1.977(1)	
	Mn-O_2	2.213(1)	
		1.893(1)	
		1.881(1)	

the combination of electronegative and Jahn-Teller effect of central coordinated ion should be the main reasons for the smallest bulk modulus of manganite among InOOH-related structural hydroxides.

5 CONCLUSION

The angle dispersion X-ray diffraction technology has been employed to obtain the *P-V* data of natural manganite up to 12.7 GPa. A third-order Birch-Murnaghan equation of state was used to fit the *P-V* data, obtained the zero-pressure volume, the isothermal bulk modulus and its pressure derivative: $V_0 = 135.46(4)$ Å^3, $K_0 = 86(2)$ GPa, $K'_0 = 6.8(6)$, and the axial elastic parameters: $K_{a0} = 93(4)$ GPa, $K_{b0} = 62(5)$ GPa, $K_{c0} = 82(4)$ GPa (based on $P2_1/c$ setting). The manganite shows obvious compression anisotropy with *b*-axis >*c*-axis >*a*-axis. We compared the compressional property of manganite with pyrolusite and other InOOH-related hydroxides, and inferred that the combination of hydrogen bonds and Jahn-Teller effect are the possible reasons for the far smaller bulk modulus in manganite than that of pyrolusite. In addition, the two main reasons for the smallest bulk modulus of manganite in InOOH-related hydroxides: first, the Jahn-Teller effect of Mn^{3+} in manganite; second, the central coordinated ion Mn^{3+} has the least electronegative in manganite.

ACKNOWLEDGEMENTS

This work is supported by the National Natural Science Foundation of China (Grant Nos. 41374107 and 41274105) and the Youth Innovative Technology Talents program of Institute of geochemistry, Chinese Academy of Sciences (2013, to Dawei Fan).

REFERENCES

[1] Bolotina N., Molchanov V., Dyuzheva T., Lityagina L., Bendeliani N. Crystallogr. Rep. 53 (2008) 960.
[2] Kohler T., Armbruster T., Libowitzky E. J. Solid State Chem. 133 (1997) 486.
[3] Suzuki A. J. Miner. Petrol. Sci. 108 (2013) 295.
[4] Garrido M. Bull. Soc. Franc. Mineral. Crystallogr. 58 (1935) 224.
[5] Buerger M. Z. Kristallogr. 95 (1936) 83.
[6] Buerger M. Z. Kristallogr. 95 (1936) 163.
[7] Dachs H. Z. Kristallogr. 118 (1963) 303.
[8] Ohtani E., Litasov K., Suzuki A., Kondo T. Geophys. Res. Lett. 28 (2001) 3991.
[9] Ohtani E., Sano A., Sakai T., Kondo T. Photon Factory Activity Report 13A (2007) 2005G151.
[10] Sano A., Ohtani E., Kondo T., Hirao N., Sakai T., Sata N., Ohishi Y., Kikegawa T. Geophys. Res. Lett. 35 (2008) L03303.
[11] Tsuchiya J., Tsuchiya T., Tsuneyuki S., Yamanaka T. Geophys. Res. Lett. 29 (2002) 1909.

[12] Xu Ja., Hu J., Ming Lc., Huang E., Xie H. Geophys. Res. Lett. 21 (1994) 161.
[13] Friedrich A., Wilson D., Haussühl E., Winkler B., Morgenroth W., Refson K., Milman V. Phys. Chem. Miner. 34 (2007) 145.
[14] Vanpeteghem C., Ohtani E., Kondo T. Geophys. Res. Lett. 29 (2002) 1119.
[15] Vanpeteghem C., Ohtani E., Kondo T., Takemura K., Kikegawa T. Am. Mineral. 88 (2003) 1408.
[16] Ohtani E. Elements 1 (2005) 25.
[17] Mao H. K., Bell P. M., Shaner J. W., Steinberg D. J. J. Appl. Phys. 49 (1978) 3276.
[18] Anderson O., Isaak D., Yamamoto S. J. Appl. Phys. 65 (1989) 1534.
[19] Hammersley J. (1996) Fit2D report. European Synchrotron Radiation Facility, Grenoble, France
[20] Post J. Proc. Nat. Acad. Sci. 96 (1999) 3447.
[21] Holland T., Redfern S. Miner. Mag. 61 (1997) 65.
[22] Birch F. Phys. Rev. 71 (1947) 809.
[23] Angel R. (2001) EOS-FIT V5.2 computer program. Crystallography Laboratory, Department of Geological Sciences, Virginia Tech, Blacksburg, VA, USA
[24] Angel R. Rev. Miner. Geochem. 41 (2000) 35.
[25] Fan D., Ma M., Zhou W., Wei S., Chen Z., Xie H. Phys. Chem. Miner. 38 (2011) 95.
[26] Hwang G., Post J., Lee Y. Phys. Chem. Miner. 42 (2015) 405.
[27] Hazen R., Finger L. J. Geophys. Res. 84 (1979) 6723.
[28] Shannon R. Acta. Crystallogr. A 32 (1976) 751.
[29] Dewhurst J., Lowther J. Phys. Rev. B 64 (2001) 014104.
[30] Haines J., Léger J., Hoyau S. J Phys. Chem. Solids 56 (1995) 965.
[31] Li Y., Wu X., Qin S., Wu Z. Chin. J. High Press. Phys. 20 (2006) 285.
[32] Baur W. Acta Crystallogr. B 32 (1976) 2200.
[33] Smyth J., McCormick T. (1995) Crystallographic data for minerals. In: Ahrens T. (ed.) Mineral physics and crystallography: a hand book of physical constants, American Geophysical Union, Washington, D. C., pp 1–17.
[34] Xu J., Ma M., Wei S., Hu X., Liu Y., Fan D., Xie H. Phys. Chem. Miner. 41 (2014) 547.
[35] Wei S., Ma M., Fan D., Yang J., Zhou W., Li B., Chen Z., Xie H. High Pressure Res. 33 (2013) 27.
[36] Nagai T., Kagi H., Yamanaka T. Am. Mineral. 88 (2003) 1423.
[37] Yang H., Lu R., Downs R., Costin G. Acta Crystallogr. E 62 (2006) i250.
[38] Mao H., Shu J., Hu J., Hemley R. Solid State Commu. 90 (1994) 497.
[39] Suzuki A. Mineral. Mag. 73 (2009) 479.
[40] Sano-Furukawa A., Kagi H., Nagai T., Nakano S., Fukura S., Ushijima D., Iizuka R., Ohtani E., Yagi T. Am. Mineral. 94 (2009) 1255.
[41] Sano-Furukawa A., Yagi T., Okada T., Gotou H., Kikegawa T. Phys. Chem. Miner. 39 (2012) 375.
[42] Gleason A., Jeanloz R., Kunz M. Am. Mineral. 93 (2008) 1882.
[43] Suzuki A. Phys. Chem. Miner. 37 (2010) 153.
[44] Pernet M., Berthet-Colominas C., Franco M., Christensen A. Phys. Status Solid A 43 (1977) 81.
[45] Li S., Zheng C., Lobringn K. Z. Kristallogr. 218 (2003) 11.
[46] Lehmann M., Larsen F., Poulsen F., Christensen A., Rasmussen S. Acta Chem. Scand. 24 (1970) 1662.